

CHAPTER 9

HF SKYWAVE RADAR MEASUREMENT OF HURRICANE WINDS AND WAVES

Joseph W. Maresca, Jr. and Christopher T. Carlson*

I. INTRODUCTION

We measured significant wave height, and surface wind speed and direction for the first two Gulf of Mexico hurricanes of the 1977 season using a high frequency (HF) skywave radar. The radar measurements were made from California by using the SRI-operated Wide Aperture Research Facility (WARF). We recorded sea backscatter for hurricanes Anita and Babe, at distances more than 3000 km from the WARF, by means of single F-layer ionospheric reflection. We compiled real-time maps of the surface wind direction field within a radial distance of 200 km of the storm center, then estimated the hurricane position from these radar wind maps, and developed a track for Anita over a 4 day period between 30 August and 2 September 1977 as the storm moved westward across the Gulf of Mexico. The radar track was computed from 17 independent position estimates made before Anita crossed the Mexican coast, and was subsequently compared to the official track produced by National Hurricane Center (NHC). Agreement between the WARF position estimates and coincident temporal positions on the NHC smooth track was ± 19 km. At approximately 0000Z on 1 September 1977, Anita passed within 50 km of the National Data Buoy Office (NDBO) open ocean moored buoy EB-71, and provided us with the opportunity to compare WARF estimates of the significant wave height, and surface wind speed and direction in all four quadrants of the storm with those made at the buoy. Agreement between the WARF and EB-71 measurements was within 10%.

Two days after Anita crossed land, tropical storm Babe--a weaker, short-lived storm--developed. WARF estimates of the significant wave height, and surface wind speed and direction were made for selected regions of the storm.¹ No in situ wave measurements were available for comparison to the WARF measurements. WARF estimates of the wind speed were compared to wind speed measurements made at nearby oil platforms, and surface wind speeds computed from flight level winds (305 m) measured by a NOAA reconnaissance aircraft. Agreement was again within 10%. The purpose of this paper is to describe the capability of remotely monitoring hurricanes and other open ocean storms by using an HF skywave radar. We will describe the important aspects of the WARF skywave radar, the sea echo Doppler spectra, the method of analysis used to estimate the wave and wind parameters, and the accuracy of these radar-derived quantities.

* SRI International, Menlo Park, California 94025.

II. WARF SKYWAVE RADAR

The Wide Aperture Research Facility (WARF)² is a high-resolution experimental high frequency skywave radar located in central California. The radar is bistatic and operates in the HF band between 6 and 30 MHz. Ocean areas are illuminated by a 20-kW swept-frequency continuous-wave (SFCW) signal from a transmitter site located at Lost Hills, California. The energy reflected from the surface beam is received 185 km to the north at Los Banos, California. The receiving antenna array is 2.5-km long and consists of a double linear array of 256 whip antennas producing a nominal $1/2^\circ$ azimuthal beamwidth at 15 MHz. The signal propagates to and from remote ocean patches by means of one or more ionospheric "reflections."

The coverage area is shown in Figure 1. The radar can be directed either east or west, and can be electronically steered in azimuth $\pm 32^\circ$ from boresight anywhere within the coverage area in $1/4^\circ$ increments. Position accuracy is a function of midpath ionospheric height estimates where uncertainty in the midpath height results in a nominal position accuracy of approximately 20 km. At any one location, the accuracy between consecutive measurements in range and azimuth is an order of magnitude better. WARF has multiple-beam capability, and sea backscatter is usually received simultaneously at four adjacent ocean areas from four different beams separated by $1/4^\circ$. The size of the ocean scattering patch is a function of the beamwidth, the range, the range cell separation, and the number of range cells averaged together. The size of the minimum scattering patch at a range of approximately 2000 km is 3 km in range by 15 km in cross range.

III. IONOSPHERIC PROPAGATION

The ionosphere consists of ions produced in the earth's atmosphere, primarily by solar radiation. Radio-wave propagation by means of ionospheric reflection occurs primarily between elevations of 100 km and 500 km. A graph of electron density as a function of height may show peaks in the ionospheric profile. These peaks are defined as layers and are designated by E_s (sporadic-E), E, F1, and F2. They correspond to peak electron densities located at about 110, 120, 200, and 300 km above the earth, respectively. Ionospheric conditions are transient in time and space and depend on the stability and strength of the electron density profile.³

The minimum radar range for one hop ionospheric propagation is approximately 1000 km; the maximum radar range is approximately 3000 km. The ionosphere will support propagation to a specific range over a limited frequency band. The achievable range is dependent on time of day, geographical region, and ionospheric height. We use two different types of real-time ionospheric soundings at WARF to manage the ionospheric propagation. An oblique-incidence sounding shown in Figure 2 is primarily used to determine: the relative signal strength; the radio

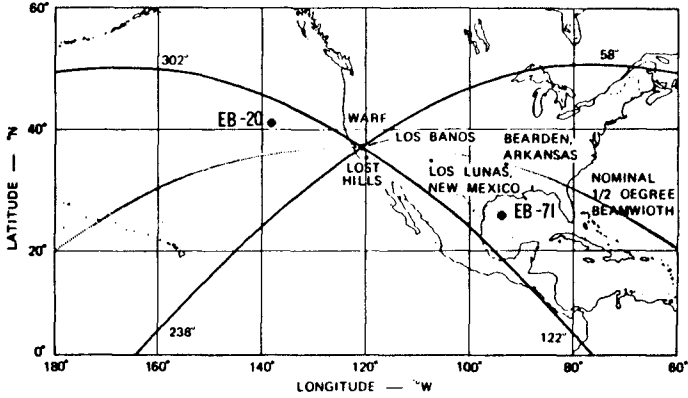


FIGURE 1 COVERAGE AREA OF THE WARF HF SKYWAVE RADAR. All Anita measurements were made west of 88° W in the Gulf of Mexico.

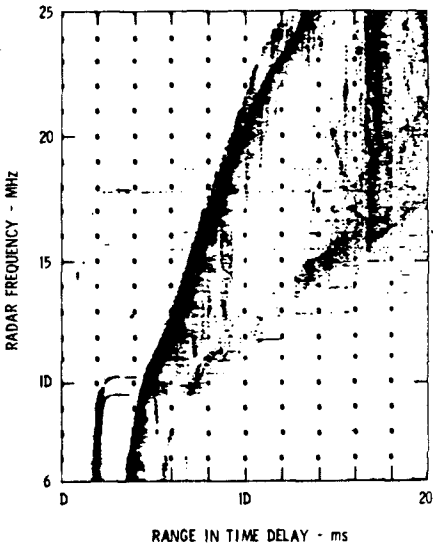


FIGURE 2 OBLIQUE-INCIDENCE SOUNDING TAKEN AT WARF. The oblique-incidence sounding is a plot of energy received for a given frequency at a given range.

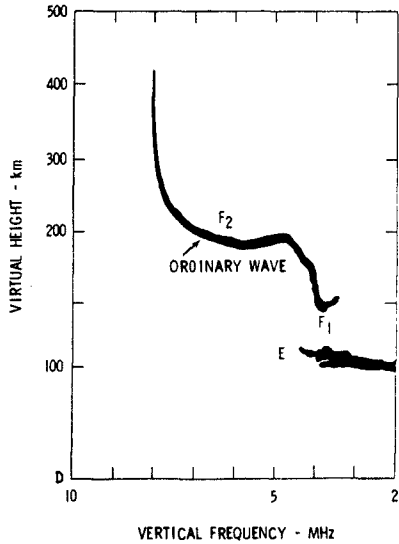


FIGURE 3 VERTICAL-INCIDENCE IONOSPHERIC SOUNDING TAKEN AT WARF. The vertical-incidence sounding is a plot of overhead energy for different frequencies.

frequencies that will propagate to a particular range; and certain types of ionospheric disturbances such as traveling waves, and focusing or defocusing of energy. A vertical-incidence sounding shown in Figure 3 taken between the WARF transmitting and receiving arrays is primarily used to measure the overhead ionospheric mode structure and height of each ionospheric layer. A frequency surveillance spectrum analyzer is used to select interference-free frequency bands.

IV. SEA ECHO DOPPLER SPECTRUM

The sea backscatter received at the WARF is coherently processed in range and Doppler to produce a sea echo Doppler spectrum. We usually process 21 independent Doppler spectra spaced at 3-km range intervals. These spectra are obtained simultaneously at each of four adjacent radar beams. A total of 84 independent Doppler spectra are obtained for each coherent time period. We compute an average spectrum from a subset of these Doppler spectra, depending on the type of measurement and the time and space scales associated with the ocean surface features. An example of a mean sea echo Doppler spectrum produced by averaging 112 spectra obtained from four consecutive 102.4 s coherent time periods, over a scattering patch consisting of 21 range cells and 3 adjacent beams is shown in Figure 4.

The sea echo Doppler spectrum shown in Figure 4 is characterized by two dominant first-order echoes surrounded by a second-order continuum. Crombie⁴ interpreted the first-order echoes in terms of simple Bragg scattering that represented a resonant response between radio waves of wave number k_0 and ocean waves of wave number $k = 2 k_0$. The radar measures the relative power and Doppler of the ocean waves traveling radially toward or away from the radar. The power ratio of the two first-order echoes are indicative of the wave direction of the waves of wave number k . Because k is usually large ($k > 0.5$), it is assumed that the wind direction is identical to the direction of these waves.

The wave height spectrum is derived from the second-order structure surrounding the first-order echoes. For hurricanes, the power in the second-order echoes is large. As the total wave energy increases, the amplitude of the second-order echoes increases as illustrated in Figure 5. Barrick^{5,6} derived theoretical expressions that accurately model the HF scattering process to second order. For a specific directional wave spectrum, the model computes the Doppler spectrum. The effects of the wind direction, wave directionality and the wave frequency spectrum on the modeled Doppler spectrum have been extensively studied by the use of this model.

V. HURRICANE DATA SAMPLING

Data sampling during a hurricane is divided into two tasks to optimize the sampling time and the data quality. The spectral resolution,

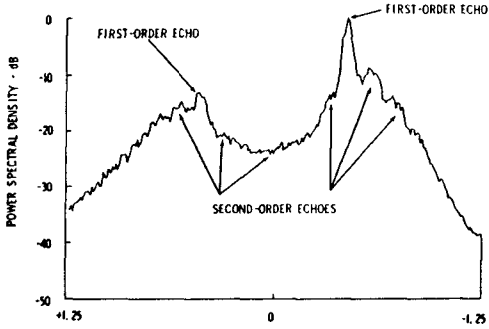


FIGURE 4 AVERAGE SEA ECHO DOPPLER SPECTRUM RECORDED WITHIN 35 km OF THE CENTER OF HURRICANE ANITA AT 2343Z ON 31 AUGUST 1977.

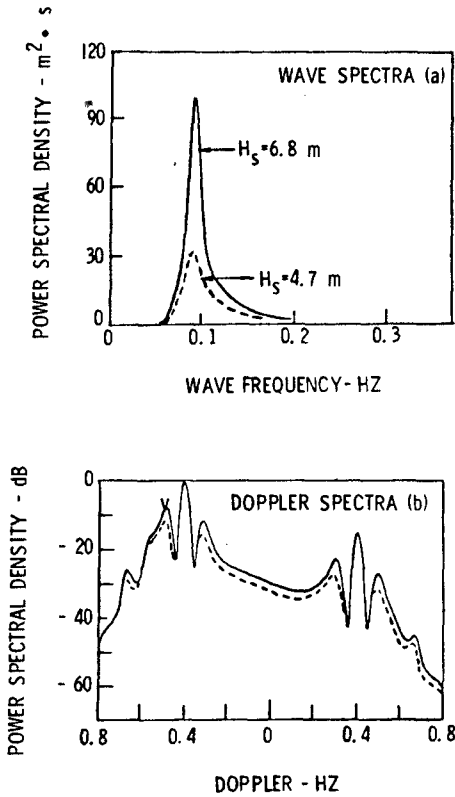


FIGURE 5 Example of Two Synthetic Doppler Spectra (b) Produced from Two Input Wave Spectra (a) With the same Directional Distribution and Radar-to-Wind Direction, but Different Total Wave Energy (0.02 Hz Resolution).

directly related to the coherent integration time, can be much coarser for first-order measurements than for second-order measurements. Wind direction estimates are computed from the first-order echoes, and can be computed considerably more rapidly than wave height and wind speed estimates, which are computed from the second-order echoes. Usually, the longer the coherent integration time, the greater the influence the ionosphere has on the quality of the data.

The quality of the recorded sea backscatter depends on the ionospheric conditions over short periods on the order of minutes. High-quality sea backscatter is obtained if the radio waves propagate by means of a strong, single, stable, coherent ionospheric layer. Sometimes the signals may be received at the same time from two or more different paths (multipath). In this case, the second or succeeding signals will be reflected from different parts of the ocean and different parts of the ionosphere, and will contaminate the sea echo received from the first path. If the ionosphere is changing in time or space during the coherent radar dwell (time period), further degradation of the data will occur. The ability to predict the ionospheric conditions would enable the radar operator to minimize the contaminating effects of the ionosphere, improve the quality of sea backscatter, and reduce the sampling time. The ionospheric soundings provide some data quality information. The vertical and oblique incidence soundings are taken every 10 minutes; a complete sounding requires approximately 3 minutes. The coherent radar measurements made at WARF require between 10 and 100 seconds to complete. Because the time it takes to complete a sounding is greater than the time required to record the sea backscatter data, assessment of the data quality is difficult for rapidly changing ionospheres. Therefore, real-time output of the data from the WARF site minicomputer is used to verify data quality.

The wind direction measurement is not extremely sensitive to ionospheric contamination caused by multipath or smearing because only the amplitude of the two strong first-order echoes must be measured. Coherent integration times of 12.8 seconds (0.078-Hz resolution) are sufficient to resolve the peaks of the first-order echoes. We can map the wind-direction field in a hurricane by scanning in range and azimuth. It is possible to routinely map the surface-wind-direction field of a hurricane and this can be accomplished in about 10 minutes. Once the surface-wind-direction map is made, the storm center can be identified for tracking purposes, and regions of interest can be selected for more extensive monitoring of wind speed and wave height anywhere within the storm.

The significant wave height and wind speed measurements are sensitive to ionospheric contamination. This contamination is the largest source of error in these measurements. A coherent integration time of 102.4 seconds (0.01-Hz resolution) is required to resolve the second-order echoes. The ionosphere does not generally support coherent integration time periods of this length. Multipath and ionospheric smearing can seriously degrade the weaker second-order echoes. Because of this

contamination, we are not able to routinely estimate wave height for each 102.4-second time period as we were able to calculate wind direction for each 12.8-second time period. A sampling strategy that combines careful propagation management through selection of frequencies, which result in a stable, coherent, single propagation path, and signal processing that minimizes the contaminating effects of the ionosphere are used to obtain a data set suitable for analysis. Recent work by SRI and NOAA⁷ has resulted in improved methods of collecting high quality data by sorting the data according to a spectral sharpness index. The effect of ionospheric contamination, however, is less severe for data recorded during large waves generated during a hurricane. The amplitude of the second-order echoes containing the wave height information may be stronger than the contamination effects, and thus, wave height can be calculated despite the contamination.

For the Anita and Babe wind direction measurements, we divided the data into 16 groups and analyzed three consecutive 12.8-second coherent radar dwells. Each wind direction estimate was calculated from a minimum of 15 Doppler spectra. At a range of 3000 km, the size of each scattering patch is 15 km × 25 km. It would be desirable to compute wave height and wind speed from a similar data set, but this is not generally possible. Longer coherent time periods and more independent samples of the spectra are required to obtain a high quality sample. We could collect the data over a small scattering patch by averaging over a long time, or we could increase the scattering patch size and average in space. Averaging in space is preferable because it reduces the total time required to obtain a mean Doppler spectrum. For the Anita and Babe wave height and wind speed measurements, we analyzed the data from three of the adjacent azimuth cells and 21 contiguous range cells. The total scattering patch is 63 km × 50 km. Several consecutive integration periods are required to record the data.

VI. WIND DIRECTION MEASUREMENT

HF skywave radar has been used to map the surface-wind fields associated with large weather systems⁸ and tropical storms.⁹ The radar measured surface-wind directions are derived from the predominant direction of ocean gravity waves, approximately 10-m long. The waves satisfying the first-order Bragg scattering condition, $k = 2k_0$, are assumed to be tightly coupled to the wind for time scales on the order of tens of minutes. This assumption is reasonable for the high wind speed conditions associated with hurricanes. Available directional wave spectra measurements¹⁰⁻¹² indicate that the dominant wave direction is representative of the predominant wind direction. For open ocean conditions, agreement between the WARF radar and shipboard anemometer measurements of wind direction is $\pm 16^\circ$ ¹³. For hurricane winds, the agreement between coincident wind direction measurements made by the NOAA National Data Buoy Office (NDBO) data buoys and the WARF radar is better than 10° ^{1,9}.

The radar measures the relative power between the approaching and receding waves that satisfies the Bragg scattering condition. If a cosine directional distribution¹⁰

$$G(\theta) = \cos^s \theta / 2 \quad (1)$$

is assumed, then the relative power of the approaching and receding waves measured by the radar is sufficient to estimate θ with an ambiguity about the beam direction. This left-right ambiguity is resolved by the predictable cyclonic surface circulation within the hurricane. The shape of $G(\theta)$ is controlled by the spreading parameter, s , where θ is the angle between the radar beam and the wind direction. For open ocean conditions, we have estimated s from several models.^{11,13} For the maximum hurricane winds, the values of s estimated from these models are too low. Based upon previous hurricane analyses and spot measurements of wind direction at NDBO data buoys, we used values of s between 1.0 and 2.0. No attempts were made to account for variations in s as a function of location within the hurricane.

VII. SIGNIFICANT WAVE HEIGHT

Barrick⁶ derived an integral expression that predicts the Doppler spectrum for a specific directional wave spectrum input. Recent efforts have succeeded in inverting this integral expression to compute the input rms wave height,^{14,15} one-dimensional wave frequency spectrum,¹⁶⁻¹⁹ and the directional distribution.¹⁷⁻¹⁹ Barrick's^{14,16} expressions have been used to analyze skywave radar data recorded for a Pacific Ocean storm¹⁵ and tropical storms.^{1,20}

We used a power law derived from simulated data by Maresca and Georges¹⁵ to compute rms wave height by relating the ratio of the total second-order and first-order power to the rms wave height:

$$k_0 h = a R_2^b \quad (2)$$

where $0.2 \leq k_0 h \leq 1.0$, h is the rms wave height; k_0 is the radar wave number; R_2 is the ratio of the total second- to total first-order power; and $a = 0.8$ and $b = 0.6$ are constants. This average expression was derived from theoretical simulations of the Doppler spectra for different radar-to-wind directions, directional distributions, functional forms of the wave frequency spectrum, and operating radar frequencies. Equation (2) is accurate to within 10%. Discussion of the errors can be found in Maresca and Carlson,¹ and Maresca and Georges.¹⁵

VIII. WIND SPEED

Historically, wave models have been developed to predict wave height and the wave spectrum from an input wind field. The accuracy of these models is dependent upon the accuracy of the input winds. Hasselmann et al.²¹ proposed a one-dimensional parametric wind-wave model for fetch limited growing wind-sea conditions. Ross and Cardone²²⁻²⁵ empirically derived a power law expression for hurricanes based on the form proposed by Hasselmann that relates the nondimensional wave energy, \tilde{E} , by using wind, wave and fetch measured during hurricanes Ava, Camille, and Eloise. For hurricanes,

$$\tilde{E} = 2.5 \times 10^{-5} \tilde{R}^{0.45} \quad (3)$$

where $\tilde{E} = E g^2 / W^4$; $\tilde{R} = r g / W^2$; $E = h^2$; and $H_s = 4h$. In \tilde{E} and \tilde{R} , E is the total wave energy; h is the rms wave height; H_s is the significant wave height; r is the radial distance from the eye to the measurement point that accounts for fetch; g is the gravitational acceleration; and W is the wind speed. Solving for wind speed in Eq. (3), we obtain

$$W = \left(\frac{h^2 g^2}{2.5 \times 10^{-5} (r g)^{.45}} \right)^{0.323} \quad (4)$$

The wind-wave model used to derive Eq. (4) is applicable for slow moving storms in which $W > 15$ m/s and $\tilde{R} < 3 \times 10^4$. For the unusual cases where the storms move very fast or very slow, Ross and Cardone²⁴ showed that significant differences in the modeled and measured wave heights occur.

We used Eq. (4) to calculate wind speed for both Anita and Babe and compared our results with the wind speeds measured at NDBO buoys, oil platforms, and by reconnaissance aircraft. The radial fetch (r) was measured from the WARF-derived wind maps, and the wave height (h) was computed using Eq. (2). The radar-derived W is not an instantaneous wind speed estimate; it is a smooth temporal and spatial average of the winds. Our radar-derived W was compared to the 15-minute wind speed averages made at NDBO moored data buoys.

IX. ANITA MEASUREMENTS

Hurricane Anita formed as a tropical depression in the Gulf of Mexico at about 1200Z on 29 August 1977. Anita developed into a tropical storm at approximately 0600Z on 30 August 1977, and about 12 hours later intensified into the first Gulf of Mexico hurricane of the 1977 season. As Anita moved west across the Gulf, winds in excess of 75 m/s were recorded. Five days of skywave data beginning on 29 August 1977 were recorded prior to Anita's landfall on 2 September 1977 approximately 48 km south of Brownsville, Texas. Twenty-one radar wind maps were compiled at WARF. The first 4 wind maps were not used in the

radar-derived track presented here because the radar showed two distinct centers during this early period. On 30 August 1977, the storm intensified and developed one center. The wind maps were updated 3 to 5 times per day during both daytime and nighttime periods and were used to develop the WARF-derived track. Figure 6 shows the radar-derived positions in relation to the official NHC smooth track produced from reconnaissance aircraft measurements, visible and infrared satellite cloud photographs, and shore-based microwave Doppler radar. The relative agreement between the WARF position estimates and the interpolated temporal position estimates along the smooth track is ± 19 km.

There are two principal errors associated with the WARF hurricane position fixes: the absolute position error of the radar and the errors associated with locating the storm center from the radar wind direction measurements. We estimate the range errors of the radar caused by errors in determining the ionospheric height at midpath to be 20 km. If a coastal scan is included as part of collecting the wind map data, the land echo can be used as a reference to more accurately determine the ionospheric height, and therefore, reduce this error. We estimate the error in azimuth caused by ionospheric tilting to be 20 km. These range and azimuth errors can be reduced significantly by installing an HF repeater along the coast which receives our signal and transmits it back with a known frequency shift. Assuming similar mean ionospheric conditions within 200 km of the storm center, the entire wind map can be translated in azimuth and range to correct for the absolute position error. The location of the wind direction measurement with respect to the storm center is generally not affected by these position errors. We estimate the error associated with determining the storm center from the radar maps to be 20 km. The error is caused by the left/right ambiguity in the wind direction measurement. We can expect a maximum error of about 40 km from these two sources of error. In comparing the WARF position fixes to the NHC track we found relative differences of between 5 and 50 km. We attribute these relative differences to the above sources of error.

Anita passed 50 km south of NDBO buoy EB-71 at about 0000Z on 1 September 1977. Two WARF-derived wind maps were made at 2140Z on 30 August 1977 and 0120Z on 1 September 1977 that bracket this time period. One of these wind maps is shown in Figure 7. Also shown on Figure 7 are surface wind direction fields derived from data recorded by NDBO buoy EB-71. These buoy-measured wind directions were recorded at 2-hour intervals during the period ± 18 hours of Anita's passing EB-71. The buoy-derived wind field was computed by a time-space conversion that assumed uniform wind direction and lateral storm motion during this period. We compared the buoy-derived wind directions to the WARF-derived wind directions; agreement was within 19° . Agreement between the WARF-derived wind direction estimate coincident in time and space with the buoy wind direction estimate was 1° .

Between 2314Z on 31 August 1977 and 0020Z on 1 September 1977, WARF measurements were made at five locations surrounding the center of the

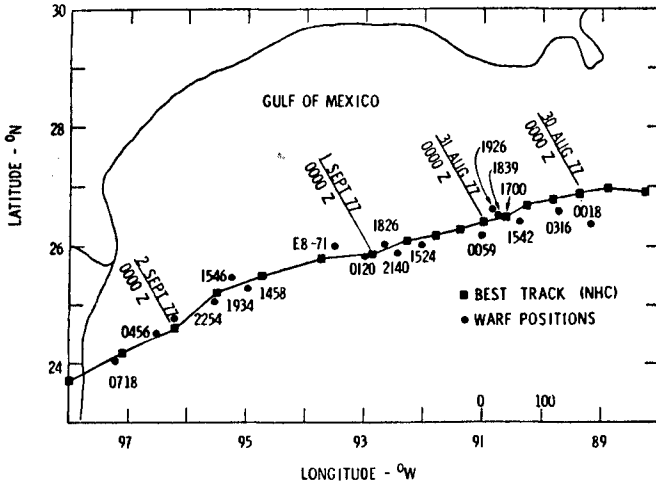


FIGURE 6 WARF-Measured Track of Hurricane Anita produced from the Radar Wind Maps

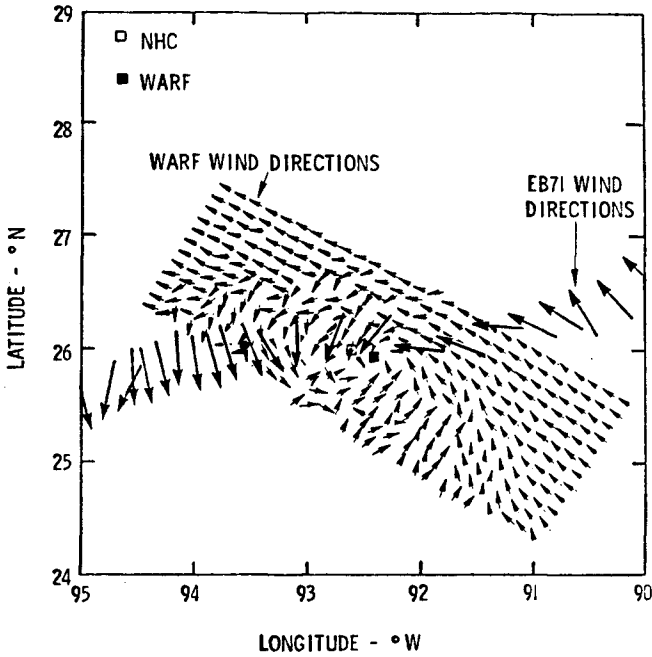


FIGURE 7 WARF-Derived Wind Direction Map made for Anita at 2140Z on 31 August 1977.

storm. The location of each measurement relative to the storm center was interpolated from the two wind maps. We computed the wind direction by using Eq. (1), wind speed by using Eq. (4), and wave height by using Eq. (2) at each location (see Table 1), and compared these measurements to a buoy-derived wind and wave field. The maps of the spatial distribution of the wind direction, wind speed, and wave height were compiled from NDBO EB-71 data buoy measurements. Each parameter was plotted in relation to the storm center and is shown in Figures 8, 9, and 10. We assumed that Anita moved uniformly with no change in the meteorological conditions during the period 18 hours before and 18 hours after passing the buoy.

Table 1
WARF ESTIMATES OF SIGNIFICANT WAVE HEIGHT,
WIND SPEED, AND WIND DIRECTION

| Point | Lat (°N) | Long (°W) | Time (GMT) | r* (km) | N* | H _s * (m) | W* (m/s) | φ* (°N) |
|-------|-------------|--------------|---------------|------------|-----|-------------------------|-------------|------------|
| A | 25.7 | 92.9 | 2314 | 35 | 80 | 5.8 | 26.7 | 277.5 |
| A | 25.7 | 92.9 | 2343 | 35 | 112 | 5.2 | 22.8 | - |
| B | 26.3 | 92.1 | 2324 | 75 | 80 | 6.0 | 24.4 | 95.1 |
| C | 26.3 | 93.1 | 2358 | 65 | 35 | 5.8 | 24.4 | 70.2 |
| D | 25.7 | 92.1 | 0003 | 65 | 134 | 5.1 | 22.5 | 168.8 |
| E | 25.2 | 91.1 | 0020 | 180 | 49 | 4.6 | 18.1 | 137.2 |

*
r = Radial Distance
N = Number of Spectra Averaged
H_s = Significant Wave Height
W = Wind Speed
φ = Wind Direction

The significant wave height shown in Figure 8 was measured at the buoy every 3 hours; the wind direction and wind speed shown in Figures 9 and 10, were measured at the buoy every 2 hours. During this 36-hour period, Anita began to intensify, and the validity of the buoy-derived wind and wave fields are suspect. Exact comparison of the EB-71 and WARF measurements are difficult because of the differences in the time, location, and area of ocean monitored. On Figure 8 we also included the wave hindcast for significant wave height computed by Cardone et al.²⁵ for comparison.

The WARF estimates made at Point B (26.3°N, 92.1°W) are in close proximity to the buoy-derived estimates located at (26.2°N, 92.1°W). The remaining WARF wind and wave height estimates are too far away from the buoy-derived quantities for direct comparison, but the agreement between the WARF- and buoy-derived wind and wave fields is reasonable.

The wave hindcast was compared to both the buoy- and WARF-derived wave heights. We find good agreement between the hindcast, buoy and WARF estimates of wave height along the 4.6-m contour east of the hurricane. The buoy estimate west of the hurricane along the 4.6-m contour line suggests the radius of this contour line is too large. WARF estimates of wave height at Points B and C, located at the extremes of the hindcast region of highest waves, are lower than the hindcast. The good agreement of Point B with the nearby buoy estimate, and the consistency of the WARF estimates at Point B and C suggest that the 7.6-m contour should be smaller. The WARF estimates of wave height at Points A and D are located between the 6.1-m contours. Again the buoy- and WARF-derived wave heights suggest that the 6.1-m contour line is too large. We should also note that any contamination of the sea echo Doppler spectra by the ionosphere would result in radar wave-height estimates that would be too high. The composite of wave height data obtained from the hindcast and EB-71 buoy indicate the validity of the WARF wave height estimates.

The agreement between the WARF-derived estimates of wind speed and the buoy-derived estimates of wind speed is good. There are three principal errors associated with the WARF wind speed estimate: error in estimating the radial fetch, error in estimating the rms wave height and error in the parametrics model. We computed the error in calculating wind speed for a ± 0.5 m error in estimating wave height for a significant wave height of 5.5 m (9.1% error) for radial fetches of 30, 50, 70 and 100 km. The errors were less than 1.6 m/s. We also computed the error in calculating wind speed for a ± 20 km error in estimating the radial fetch for a significant wave height of 5.5 m and radial fetches of 30, 50, 70, and 100 km. For radial fetches greater than 30 km, a +20 km error causes an error of less than 2 m/s in wind speed. For radial fetches greater than 50 km, a -20 km error causes an error of less than 2 m/s in wind speed. This represents less than an 8% error. These errors are typical of the WARF estimates of the significant wave height and radial fetch measurements. The errors associated with the model are discussed in Ross and Cardone.²⁴ For Anita, the mean and rms differences between the Cardone et al.²⁵ parametric model forecast and measured wave heights at EB-71 is 0.21 ± 0.83 m. This includes errors in measuring wave height at the buoy and radial fetch from the conventional position fixes. We also calculated the wind speed using Eq. (4) for some of the buoy-measured wave heights shown in Figure 8, and compared the calculated wind speed measurements to wind speeds measured at the buoy (Table 2). The data is indicative of the accuracy we could expect from the WARF estimates of wind speed using Eq. (4). For these data, we believe the largest sources of error in the comparison are the uncertainty in the radial distance to each point caused by compiling the map over a 36-hour period, and the assumption of a symmetrical distribution of the winds.

Table 2

COMPARISON OF WIND SPEED VALUES CALCULATED
FROM EQ. (4) DERIVED FROM EB-71 SIGNIFICANT
WAVE HEIGHT MEASUREMENTS

| Lat (°N) | Long (°W) | H_S^* (m) | r^* (km) | W_C^* (m/s) | W_m^* (m/s) | Difference (m/s) |
|-------------|--------------|----------------|---------------|------------------|------------------|---------------------|
| 25.5 | 94.8 | 2.5 | 217 | 11.9 | 7.6 | +4.3 |
| 25.7 | 94.4 | 2.9 | 174 | 13.5 | 9.0 | +4.5 |
| 25.7 | 93.9 | 3.1 | 124 | 14.9 | 13.3 | +1.6 |
| 25.8 | 93.4 | 5.5 | 69 | 23.4 | 17.4 | +6.0 |
| 26.0 | 92.5 | 6.5 | 24 | 30.4 | 34.1 | -3.7 |
| 26.3 | 91.5 | 4.7 | 126 | 19.4 | 23.1 | -3.7 |
| 26.6 | 90.7 | 4.6 | 212 | 17.7 | 18.1 | -0.4 |

*
 H_S = Significant Wave Height
 r = Radial Distance
 W_C = Computed Wind Speed
 W_m = Measured Wind Speed

X. BABE DATA

We recorded skywave data for Babe from 2000Z on 4 September 1977 until landfall on 5 September 1977. Wind direction maps were made at 2253Z on 4 September 1977 and 1507Z on 5 September 1977. Babe was already onshore before the second map was made. We analyzed a sea echo Doppler spectrum near the peak winds for wind speed. This spectrum was recorded at a radius of 50 km from the hurricane center (27.9°N, 91.6°W). The WARF estimate of significant wave height was 3.6 m. The wind speed was computed by using Eq. (4) and was compared to wind speeds measured at several offshore oil platforms at 2100Z and from aircraft reconnaissance at 1800Z. Winds measured from aircraft at an altitude of 305 m were reduced to the equivalent 10 m wind for comparison to the radar data. We reduced the aircraft winds to the surface using a simple ratio relating upper level gradient wind to the surface wind, indicated by Elsberry et al.²⁶ calculations. Using the two layer Cardone²⁷ marine boundary layer model, Elsberry et al.²⁶ computed the ratio of the wind at the top of the upper layer to the wind at the top of the surface layer for different regions of the hurricane, different surface roughness and different ratios of heat conductivity to eddy viscosity. For moderate to high wind speeds, the top of the surface layer is approximately 20 m. This wind ratio ranges from about 0.5 to 0.85. The lower value represents regions near the peak winds. We assumed the 305 m aircraft wind was representative of the wind at the top of the upper layer and reduced it to 20 m using a ratio of 0.6. The corrected 20 m wind is 18.5 m/s. We realize the error associated with this calculation can

be large. We computed the 19.5 m WARF wind speed for comparison by assuming a logarithmic profile in the surface boundary layer of the form

$$W(z) = \frac{W_*}{k} \ln \left(\frac{z}{z_0} \right) \quad (5)$$

where $W(z)$ is the wind speed at a height of z , $W_* = C_D W^2$ is the friction velocity, C_D is the drag coefficient, $k \approx 0.4$ is Von Karman's constant, and z_0 is the surface roughness. We estimated $z_0 = 0.00392$ m for hurricane conditions using the wind speeds measured during Eloise²⁸ at NDBO buoy EB-10 at 10 m, and a constant drag coefficient of 0.0026 proposed by Wu²⁹ for high wind speeds to calculate W_* . We found good agreement between our 19.5 m computed wind speed using Eq. (5) for Eloise and the 19.5 m Eloise wind speed computed by Ross and Cardone.²⁴ Using $z_0 = 0.00392$ m and $C_D = 0.0026$ m we computed the 19.5 m WARF Babe wind speed to be 18.3 m/s. We also computed the maximum wind speed, W_{\max} , and the maximum sustained wind speed, W_s , for a storm moving at 5.1 m/s from the following expressions³⁰ relating the central pressure and radius of the storm to wind speed at 10 m:

$$W_{\max} = 0.868 [6.45(P_n - P_o)^{1/2} - 0.296 rf] \quad (6)$$

and

$$W_s = 0.865 W_{\max} + 0.5 V_F \quad (7)$$

where W_{\max} and W_s are in m/s, P_n is the normal pressure of 1013 mb, P_o is the central pressure in mb, r is the radius in km, f is the coriolis parameter in radians/hour, and V_F is the forward motion of the storm in m/s. The maximum wind recorded from the aircraft at 1800Z were located approximately 60 km from the center and the central pressure was reported as 1000 mb. We calculated $W_{\max} = 16.4$ m/s and $W_s = 16.8$ m/s. We summarize these wind speed estimates in Table 3. Because none of the wind speed estimates are coincident in time or space with the WARF estimate and the assumptions inherent in deriving these quantities we can only compare the results qualitatively. The WARF wind speed estimate is reasonable.

XI. SUMMARY

Spatially-averaged hurricane wind speed, wind direction, and wave height estimates made at the WARF for Anita and Babe were compared to point measurements made at NDBO buoys and oil platforms and by reconnaissance aircraft. Agreement was within the nominal measurement accuracy of all the sensors. The WARF data set is not limited to the results presented in this paper. Other analyses of the radar data that were not obtained in the vicinity of the buoy are also available. These

experiments indicate that during a hurricane, HF skywave radar can provide operational surface data that are as accurate as the more recognized in situ measurements. The supportive surface data supplied by the WARF radar would prove particularly useful for tracking during early formative stages of hurricanes when multiple centers may be observed or when cirrus shielding may obscure visual location by satellite cloud photography. The high resolution, large coverage area, real-time steering and continuous monitoring capabilities are unique to skywave radar. The hurricane data obtained from skywave radar complements data obtained from satellites, aircraft, and buoys.

Table 3
BABE WIND SPEED ESTIMATES MADE ON 4 SEPTEMBER 1977

| Sensor | Observation (GMT) | Bearing From Hurricane Center (°N) | Radial Distance From Hurricane Center (km) | Wind Speed (m/s) |
|--------------------------------------|----------------------|--|---|------------------------|
| WARF (10 m) | 2253 | 340 | 60 | 18.2 |
| WARF (19.5 m) | 2253 | 340 | 60 | 18.3 |
| Aircraft (305 m) | 1800 | 25 | 60 | 30.8 |
| Aircraft (19.5 m) | 1800 | 25 | 60 | 18.5 |
| Oil Platform (19.5 m) | 2100 | 320 | 100 | 15.4 |
| Oil Platform (19.5 m) | 2100 | 0 | 35 | 11.3 |
| W _{CM} ¹ (9.1 m) | - | - | 60 | 16.4 |
| W _{CS} ² (9.1 m) | - | - | 60 | 16.8 |

¹Computed maximum wind speed from Eq. (3-35) in Reference 30.

²Computed maximum sustained wind speed from Eq. (3-34) in Reference 30.

Acknowledgments. This work was supported by the Air Force of Scientific Research (AFOSR) under Contract No. F49620-76-C-0023. We gratefully acknowledge the help of G. Glassmeyer, W. Preuss, G. Tomlin, and C. Powell of SRI in collecting data at WARF; D. Westover for writing the real-time sampling software; and B. Richards and J. King for typing the manuscript.

REFERENCES

1. J. W. Maresca, Jr. and C. T. Carlson, "Tracking and Monitoring Hurricanes by HF Skywave Radar over the Gulf of Mexico," Technical Report 1, SRI International, Menlo Park, California (1977).
2. "SRI Remote Measurements Laboratory Research Capabilities," brochure, Stanford Research Institute, Menlo Park, California (1977).
3. K. Davies, Ionospheric Radio Propagation, NBS Monograph 80, U.S. Government Printing Office, Washington, D.C. (1965).
4. D. D. Crombie, "Doppler Spectrum of Sea Echo at 13.56 mc/s," Nature, Vol. 175, pp. 681-682 (1955).
5. D. E. Barrick, "First-order Theory and Analysis of MF/HF/VHF Scatter From the Sea," IEEE Trans. Antennas and Propagation, AP-20, pp. 2-10 (1972).
6. D. E. Barrick, "Remote Sensing of Sea State by Radar," Remote Sensing of the Troposphere, V. E. Derr, ed., U.S. Government Printing Office, Washington, D.C. (1972).
7. T. M. Georges and J. W. Maresca, Jr., "The Effect of Radar Beamwidth on the Quality of Sea Echo Doppler Spectra Measured with HF Skywave Radar," accepted by Radio Science.
8. J. R. Barnum, J. W. Maresca, Jr., and S. M. Serebreny, "High-Resolution Mapping of Oceanic Wind Fields with Skywave Radar," IEEE Trans. on Antennas and Propagation, AP-25, pp. 128-132 (1977).
9. J. W. Maresca, Jr. and J. R. Barnum, "Remote Measurements of the Position and Surface Circulation of Hurricane Eloise by Skywave Radar," accepted by Monthly Weather Review.
10. M. S. Longuet-Higgins, D. E. Cartwright, and N. D. Smith, "Observations of the Directional Spectrum of Sea Waves Using Motions of a Floating Buoy," Ocean Wave Spectra, pp. 111-136, Prentice-Hall: Englewood Cliffs, New Jersey (1963).
11. H. Mitsuyasu, F. Tasai, T. Suhara, S. Mizuno, M. Ohkusu, T. Honda, and K. Rikiishi, "Observations of the Directional Spectrum of Ocean Waves Using a Clover Leaf Buoy," J. Phys. Oceanog., Vol. 5, No. 4, pp. 750-760 (1975).
12. J. A. Ewing, "Some Measurements of the Directional Wave Spectrum," J. Marine Research, Vol. 27, pp. 163-171 (1969).
13. R. H. Stewart and J. R. Barnum, "Radio Measurements of Oceanic Winds at Long Ranges: An Evaluation," Radio Science, Vol. 10, pp. 853-857 (1975).
14. D. E. Barrick, "Extraction of Wave Parameters from Measured HF Sea-Echo Doppler Spectra," Radio Science, Vol. 12, pp. 415-424 (1977).
15. J. W. Maresca, Jr. and T. M. Georges, "HF Skywave Radar Measurement of the Ocean Wave Spectrum," submitted to J. Geophys. Research.
16. D. E. Barrick, "The Ocean Waveheight Nondirectional Spectrum from Inversion of the HF Sea-echo Doppler Spectrum," Remote Sensing of Environment, Vol. 6, pp. 201-277 (1977).
17. B. J. Lipa, "Derivation of Directional Ocean-wave Spectra by Integral Inversion of Second-order Radar Echoes," Radio Science, Vol. 12, pp. 425-434 (1977).
18. B. J. Lipa, "Inversion of Second-order Radar Echoes from the Sea," J. Geophys. Research, Vol. 83, pp. 959-962 (1977).

19. D. E. Barrick and B. J. Lipa, "Ocean Surface Features Observed by HF Coastal Ground-wave Radars: A Progress Review," Ocean Wave Climate, eds. M. D. Earle and A. Malahoff, Plenum Publishing Company (1978).
20. J. W. Maresca, Jr., "High Frequency Skywave Radar Measurements of Waves and Currents Associated with Tropical and Extra-Tropical Storms," Ocean Wave Climate, eds. M. D. Earle and A. Malahoff, Plenum Publishing Company (1978).
21. K. Hasselmann, D. B. Ross, P. Muller, and W. Sell, "A Parametric Wave Prediction Model," J. Phys. Oceanog., Vol. 6, pp. 200-228 (1976).
22. D. B. Ross, "A Simplified Model for Forecasting Hurricane Generated Waves" (Abstract), Bull. Am. Meteorol. Soc., presented at Conference on Atmospheric and Oceanic Waves, Seattle, Washington, March 29-April 2, 1976 American Meteorological Society (1976).
23. V. J. Cardone and D. B. Ross, "State of Art Wave Predictions and Data Requirements," Ocean Wave Climate, eds. M. D. Earle and A. Malahoff, Plenum Publishing Company (1978).
24. D. B. Ross and V. J. Cardone, "A Comparison of Parametric and Spectral Hurricane Wave Prediction Products," to be published in the Proceedings of "NATO Symposium on Turbulent Fluxes Through the Sea Surface, Wave Dynamics and Prediction," Marseille, France, September 12-16, 1977, Plenum Publishing Company (1978).
25. V. J. Cardone, D. B. Ross, and M. R. Ahrens, "An Experiment in Forecasting Hurricane Generated Sea States," Proceedings of the 11th Technical Conference on Hurricanes and Tropical Meteorology, Miami, Florida (December 13-16, 1977).
26. R. L. Elsberry, N. A. S. Pearson, L. B. Corngati, Jr., "A Quasi-Empirical Model of the Hurricane Boundary Layer," J. Geophys. Research, Vol. 79, pp. 3033-3040 (1974).
27. V. J. Cardone, "Specification of the Wind Distribution in the Marine Boundary Layer for Wave Forecasting," Rept. TR 69-1 Geophys. Sci. Lab., New York University NTIS No. AD702490 (1969).
28. G. W. Whithee and A. Johnson, Jr., "Data Report: Buoy Observations During Hurricane Eloise, September 19-October 11, 1975," Environmental Sciences Division, Data Buoy Office, National Oceanic and Atmospheric Administration, Bay St. Louis, Mississippi (1975).
29. J. Wu, "Wind Stress and Surface Roughness at Air-Sea Interface," J. Geophys. Research, Vol. 74, pp. 444-455 (1969).
30. U.S. Army Coastal Engineering Research Center, Shore Protection Manual, Vol. 1, U.S. Government Printing Office, Washington, D.C. (1973).